Eur. Phys. J. Special Topics **205**, 217–230 (2012)

DOI: 10.1140/epjst/e2012-01572-8

THE EUROPEAN PHYSICAL JOURNAL SPECIAL TOPICS

Regular Article

Dragon-Kings in rock fracturing: Insights gained from rock fracture tests in the laboratory

X. Lei[a]

Geological survey of Japan, National Institute of Advanced Industrial Science and Technology, AIST Central #7, Higashi 1-1-1, Tsukuba, Ibaraki 305-8567, Japan

Received 23 November 2011 / Received in final form 09 March 2012
Published online 01 May 2012

Abstract. In order to shed some lights to the "dragon-kings" concept, this paper re-examines experimental results on rock fracture tests in the laboratory, obtained from acoustic emission monitoring. The fracture of intact rocks as well as rocks containing natural structures (joints, faults, foliations) under constant stress rate loading or creep conditions is generally characterized by typical stages with different underlying physics. The primary phase reflects the initial rupture of pre-existing microcrack population in the sample or in the fault zone. Sub-critical growth dominates the secondary phase. The third phases termed nucleation phase corresponds to the initiation and accelerated growth of the ultimate fracture. The secondary and nucleation phases in both intact rock and faulted rock show power-law (of time-to-failure) increasing event rate and moment release. Samples containing planar structures such as foliations and faults demonstrate very similar features to natural earthquakes including: 1) small number of immediate foreshocks by which fault nucleation zones could be mapped; 2) the critical nucleation zone size is normally a fraction of the sample dimension; 3) a lot of aftershocks concentrated on the fault ruptured during the main event; 4) stress drop due to the main rupture is of the order from a few tens to a few hundreds MPa; 5) *b*-value drops during foreshocks and recovers during the aftershocks. All these results agree with the suggestion that laboratory measurements require no scaling but can be applied directly to the Earth to represent local fault behavior. The ultimate failure of the sample, or fracture of major asperities on the fault surface, normally lead to extreme events, i.e., dragon-kings, which has a magnitude significantly greater than that expected by the Gutenberg-Richter power-law relation in the magnitude-frequency distribution for either foreshocks or aftershocks. There are at least two mechanisms that may lead to dragon-kings: 1) The power-law increasing event rate and moment release; and 2) Hierarchical fracturing behavior resulting from hierarchical inhomogeneities in the sample. In the 1st mechanism, the final failure corresponds to the end point of the progressive occurrence of events and thus the resulted dragon-king event can be interpreted

[a]e-mail: xinglin-lei@aist.go.jp

as a superposition of many small events. While for the 2nd mechanism an event of extreme size is the result of fracture growth stepping from a lower hierarchy into a higher hierarchy on fault surface having asperities characterized by hierarchical distribution (of size or strength) rather than simple fractal distribution. In both mechanisms the underlying physics is that fracture in rocks is hard to stop beyond certain threshold corresponding to the critical nucleation zone size.

1 Introduction

Earthquakes in the crust and acoustic emission (AE) events in stressed rocks show similarities in a wide range of aspects. Thus many studies use AE as a seismicity simulation model [e.g. 1–9]. The similarities between earthquakes and AEs are involved in a number of power-laws. For a long time there is a scale gap between laboratory studies and earthquake seismology. However, this gap has been overlapped by recent developments in studies on mining-induced seismicity [10]. It is discussed that laboratory results can be applied directly to the Earth to represent local fault behavior with no scaling requirement [11].

One of the major goals of this study is to reexamine experimental results of rock fracture tests for gaining insights on the process stepping from pre-failure damaging into the dynamic fracturing on the point of view of the "dragon-king" concept which focuses on the deviations from the power-laws. This paper focuses on two power-laws: the *Gutenberg and Richter* relationship in magnitude-frequency distribution of events and the accelerated moment release (AMR) prior to large earthquakes and rock failures. The former power law is used to identify extreme events, whereas the later law provides a possible mechanism producing the dragon-king events.

2 Power-laws in earthquakes and acoustic emissions

2.1 Power-law in magnitude-frequency distribution

The well-known *Gutenberg and Richter* [12] relationship for earthquakes,

$$\log_{10} N = a - bM \tag{1}$$

where N is the number of events of magnitude M or greater, also works for AE events in rocks [e.g. 13–15]. The global mean of the b-value for earthquakes is ~ 1.0, and the relationship hold true for all magnitudes above a lower end cut-off magnitude which is due to detecting ability of seismic stations. However, a specified fault system or subduction zone likely produces "characteristic earthquakes". A characteristic earthquake is a repeating, large earthquake that occurs more frequently than that predicted from the power-law relationship of small earthquakes. Characteristic earthquakes, called "dragon-kings" in this issue with extreme events in other fields, may reflect somewhat different underlying mechanisms which have not yet been well addressed. The ultimate failure of rock samples subjected to differential compression in laboratory is characterized by extremely larger energy release as compared with the pre-failure microcracking, or in other words pre-failure damaging, and thus demonstrates typical dragon-king behaviors. It is thus worth re-examining some experimental results for shedding lights on the dragon-kings conception.

2.2 Power-law AMR

It is known that major earthquakes are resulted from rupture of pre-existing faults or subduction zones, which generally comprise cracks and heterogeneities at all scales from grain scale through plate scale. As a result, earthquakes do not represent pure stick-slip ruptures on the fault surface but also involve some kinds of rock fracture. Therefore, the fracturing process must be investigated at all scales [16]. Current earthquake prediction falls into two methodological groups based on their treatment of either the frictional behavior of individual faults or rock fracture within the fault zone and surrounding region. The former addresses pre-slip behavior by means of numerical simulation incorporating laboratory-derived friction laws, whereas the latter considers the statistical properties of micro-earthquakes.

Fractal or hierarchical complexities in fractures and heterogeneities of the crust, in addition to the non-linear interaction between earthquakes, lead to chaotic behaviors in earthquake occurrence. Therefore, the concept of critical point behavior has been applied to earthquakes, rockbursts, and AEs using time-to-failure analysis [e.g. 17–21]. Where, the catastrophic event is considered to be a critical phenomenon occurring at a second-order phase transition in analogy to percolation phenomena. With such considerations, the fracturing process, which shows self-organization feature, can be described mathematically by a renormalization-group scheme [22]. In the vicinity of the critical point, the variations of the energy release can be characterized by a power law of time-to-failure decorated by log-periodic oscillations [23]. Mathematically, such oscillations correspond to adding an imaginary part to the exponent of the power law [20,21].

$$\sum E(t) = A + B\,(t_f - t)^{\alpha + i\omega} \tag{2}$$

where E may be any kind of energy release rate, t_f is the failure time, A is cumulative energy release at $t = t_f$, B is negative, α and ω are constant. The log-periodic oscillations, resulted from the heterogeneities in the system, correspond to an accelerating frequency modulation as the critical time is approached. It should be noted that (2) is valid only in the region close to the critical point. However, it can be extend by employing the self-similar approximation theory [24]. Using experimental data, Moura et al. [20,21] suggested that the imaginary part of the complex exponent ω has good correlation with grain size and loading rate. Larger grain size and faster loading rate result in greater ω, which indicates longer distance of interaction.

By ignoring the oscillations in (2) the following power law of AMR is obtained:

$$\sum E(t) = A + B\,(t_f - t)^{m} \tag{3}$$

AMR has been identified for a substantial number of earthquakes and observed for years to tens of years before a main earthquake over tens to hundreds of kilometers from the future epicenter [e.g. 25,26].The Benioff strain is generally used as moment release. It has been found that typical value of m is ~ 0.3 [e.g. 27–30]. However, it is worth noting that there are many large earthquakes are not preceded by clear AMR. In contrast with natural earthquakes, AMR was better observed before the failure of brittle rocks in laboratory with $m = 0.2 \sim 0.3$ [6,31], in agreement with the typical value for natural earthquakes

2.3 AMR derived from damage laws

Under loading condition of constant stress-rate (w), the energy release rate ($\dot{E}$) evaluated by the measured AE magnitude can be derived from laboratory-derived constitutive laws of stress-aided subcritical growth of crack populations having a fractal

size distribution [32]:

$$\dot{E}(t)/\dot{E}(t=0) = (1 - t/t_f)^{l+2-2l'/2-l} (1 + wt)^l \tag{4}$$

where, l is referred to as the stress corrosion index (the exponent of the power law between the mean quasi-static rupture velocity of crack populations and the stress intensity factor [2], l' is the exponent of the power law between the mean quasi-static rupture velocity of crack populations and AE rate, the failure time t_f is defined so that c approaches infinity. Under constant stress (creep) condition ($w = 0$), Eq. (4) reduces to:

$$\dot{E}(t)/\dot{E}(0) = (1 - t/t_f)^{-m'}, \; m' = l + 2 - 2l'/2-l. \tag{5}$$

The cumulative energy release is then obtained by integrating (4) with time:

$$\sum E = \int \dot{E}dt = A + B(t_f - t)^m \quad \left(B = -\frac{1}{(1-m')t_f}, m = 1 - m'\right). \tag{6}$$

It is the same equation of AMR expressed in (3). The exponent in the power-law AMR can be linked with exponents of two another power laws related AE rate and mean crack length. In such a consideration, both event rate and moment release increase in power-law of time to failure. The AMR is the result of a cascade of small events progressively releasing the stress before a large event. At the end point, the catastrophic event is a superposition of many small events occurred progressively in a very short time like a snowslide. This is a possible mechanism producing dragon-kings in rock fractures.

3 Experiment and AE data

For reading convenience, it is helpful to present a brief review here on typical experimental systems which utilize AE hypocenter monitoring. AE technology has been greatly developed during the last 3 decades. From 1990s, one major interest of experimental studies was issues related to fracture nucleation and growth. The technology applied in the laboratory of US Geological Survey allows to stabilize the failure process by controlling axial stress to maintain a constant rate of AE at a quite low level that could be sufficiently recorded by the AE monitoring system. As a result of fast unloading, the nucleation phase, which would otherwise have taken only a few seconds, could be extended to several hour duration, and the quasi-static nucleation could be well mapped by the AE hypocenters [1,8]. By using an asymmetrical loading cell it is possible to force the final shear fracture to be initiated from some artificially determined point, at some relatively lower stress level and lower AE background, allowing detailed observation of the process zone evolution [4]. Advances in technology have lead to rapid AE waveform acquisition systems in the laboratory of Geological Survey of Japan [3], allowing new observations of rupture. The rapid AE system has an ability to record as many as 32 channels of the AE signals with no major loss of events; even for AE event rates of the order of several thousand events per second such as they are normally observed before the catastrophic failure of brittle rocks such as granites [3].

When entering the 21's century, continuous recording of full waveform of AE became possible. The first documented study is perhaps that presented by Thompson et al. [7], where continuous AE waveforms of 16 channels were sampled at a sampling frequency of 5 MHz and 14-bit resolution. Digitized data were stored onto a 40 GB circular Random Access Memory (RAM) buffer providing a 268-second segment of

continuous waveform data. A similar system has also been installed in the laboratory of Geological Survey of Japan as an additional technology for exploring details of AE evolution associated with dynamic fractures or stick-slip events.

It is worth emphasizing that, under natural stress conditions, many rocks store sufficient elastic energy to drive unstable faulting on their own and thus fault growth to proceed in a violent, uncontrolled manner after fault nucleation. Therefore, on the point of view of earthquake seismology, the high speed AE waveform recording and the continuous waveform recording technologies provide better understanding of the rupture process after fault nucleation. Major data referred in this paper are obtained by using the rapid AE waveform acquisition system at Geological Survey of Japan, in addition to a full waveform recorder which has 16 channels, up to 200 MHz sampling frequency, and 14-bit resolution. The full waveform recorder can be switched between triggering mode and continuous mode quickly during the experiment. More details of the rapid AE system can be found from [3,32]. However, it may be helpful to briefly summarize some important points here. In total, 32 piezoelectric transducers (PZTs; 1/2 MHz resonant frequency, 5 mm in diameter) were directly cemented to the sample, 50 mm in diameter and 125 mm in length. Hydraulic oil is used as the confining pressure medium. The output from all transducers was amplified by 40 dB. In addition to the waveforms, the maximum amplitudes at two specified sensors are recorded separately by another recorder of 99 dB dynamic range and used to calculate the magnitude and energy of AE events. The trigger threshold for waveform recording is about 10 times larger than the threshold for the detection of the maximum amplitude. As a result, the hypocenter data constitute a subset of the magnitude data. AE hypocenters are determined from the first P-arrival times with errors less than $1 \sim 2$ mm for fine-grained rocks and slightly greater for coarse-grained rocks [5].

The observed AE magnitude is somewhat relative due to many unknown factors such as coupling effect and sensitivity. However, the relative magnitudes can be roughly shifted to equivalent earthquake magnitudes based on calibration using Laser Doppler velocitometer and corner frequency analysis [33]. Magnitude of large events with saturated waveform record can be estimated from their wave continuation time based on scaling law between magnitude and continuation time similar with that used for small earthquakes [15]. Finally, the magnitude of the main event which has split the whole sample can be estimated following the procedure presented by McGarr and Fletcher [34]. This method was used by Thompson et al. [9] in determining magnitude of induced stick-slip event in laboratory. Seismic moment of a fault embedded in an elastic medium is given by a function of shear modulus (G) of the host medium, displacement (u), and fault surface area (A)

$$M_O = GuA. \tag{7}$$

For the case of rock sample having limited dimension under a stiff loading frame, an equivalent radius (r) for a circular asperity with elastic unloading stiffness k given by [9,35,36] can be used for calculating the fault surface area.

$$r = \frac{7\pi}{16}\frac{G}{k} \tag{8}$$

where, k can be estimated from stress-drop and displacement. At last, a moment magnitude for an equivalent earthquake can be then calculated using the scaling relation of Hanks and Kanamori [37].

$$M_W = \tfrac{2}{3}\log M_O - 6.07. \tag{9}$$

However, it is important to note that McGarr method is basically a measure of elastic energy release in ultimate failure, which is pretty much controlled by stiffness of the

loading apparatus used. It can become however large if soft apparatus is used (i.e. residual silp after the breakdown continues and achieves a big displacement). So, the obtained moment magnitude should be treated as an upper-bound. Smaller events are stopped by local heterogeneity within the sample, but the ultimate failure, which has split the whole sample, is unstoppable by this mechanism and continues until using up the excess stress stored in apparatus (hence moment can be however big). To make a fair comparison, the only way is to take the rupture dimension of the ultimate event as a lower-bound estimate of its size and to estimate its magnitude using the scaling relation between magnitude and fault rupture dimension:

$$M_W = a + b \log A \tag{10}$$

where a has a typical value of $4 \sim 4.5$ and b is close to 1 for earthquakes [38].

4 Dragon-Kings in rock fracturing

4.1 A 3-phase fracturing process of intact rocks

Experimental results, particularly that obtained under constant stress rate loading conditions, which enable dynamic failure of the sample, indicate that the evolution of pre-failure damaging process can be generally characterized by three typical phases of microcracking activity termed the primary, secondary, and nucleation phases, respectively [32]. Fig. 1 shows results of an experimental study on 3 typical granites of different grain size distributions, loaded at fast (27.5 MPa/min) and slow (2 MPa/min) stress rates. In total, 6 samples of Westerly granite (WG), Oshima granite (OG), and Inada granite (IG) were tested. WG is fine-grained and has the smallest grain size (< 1 mm). IG is a typical coarse-grained granite (grain size of ~ 5 mm in average). OG is classified into intermediate-grained rock, and has a mean grain size greater than WG and smaller than IG. Follows are a brief summary of the general features and the underlying mechanisms behind these phases.

Primary phase: Microcracking during the primary phase is related to the initial rupture of the pre-existing microcracks, rather than to the sub-critical crack growth. The pre-existing microcracks are probably healed prior to loading, and consequently the initial rupture proceeds more easily by separating the crack walls by local tensile stress than by crack growth. Since a number of mechanisms can generate the local tensile stress, and since the extension strength of every crack is much lower than the shear strength, it follows that the tensile crack predominates the primary phase. It can be well understood that the primary phase shows an increasing b value with increasing stress, because stress concentration at crack tips follows a power law of crack length and thus larger pre-existing microcracks have a higher probability to rupture at a comparatively lower stress.

Secondary phase: The typical feature of the secondary phase is a microcracking activity in which the event rate increases, with increasing stress or time, while the b value decreases from its maximum at the end of the primary phase. Average values for the maximum b value in WG, OG and IG are 1.4, 1.3 and 1.2, respectively (Fig. 1). Such results clearly correlated with the major grain size of the test sample: a comparatively larger grain size results into a lower b value. The energy release during the secondary phase appears very well consistent with the AMR model presented in 2.3. Typical values of l' and l are $2.4 \sim 3.6$ and $8 \sim 6$, respectively. These values result in $k \sim 0.75$, and thus, $m \sim 0.25$, a value in agreement with the AMR models obtained for large or intermediated earthquakes as mentioned in 2.3.

Nucleation phase: The nucleation phase corresponds to the nucleation and accelerating growth of the eventual failure of the test sample. It involves a rapidly

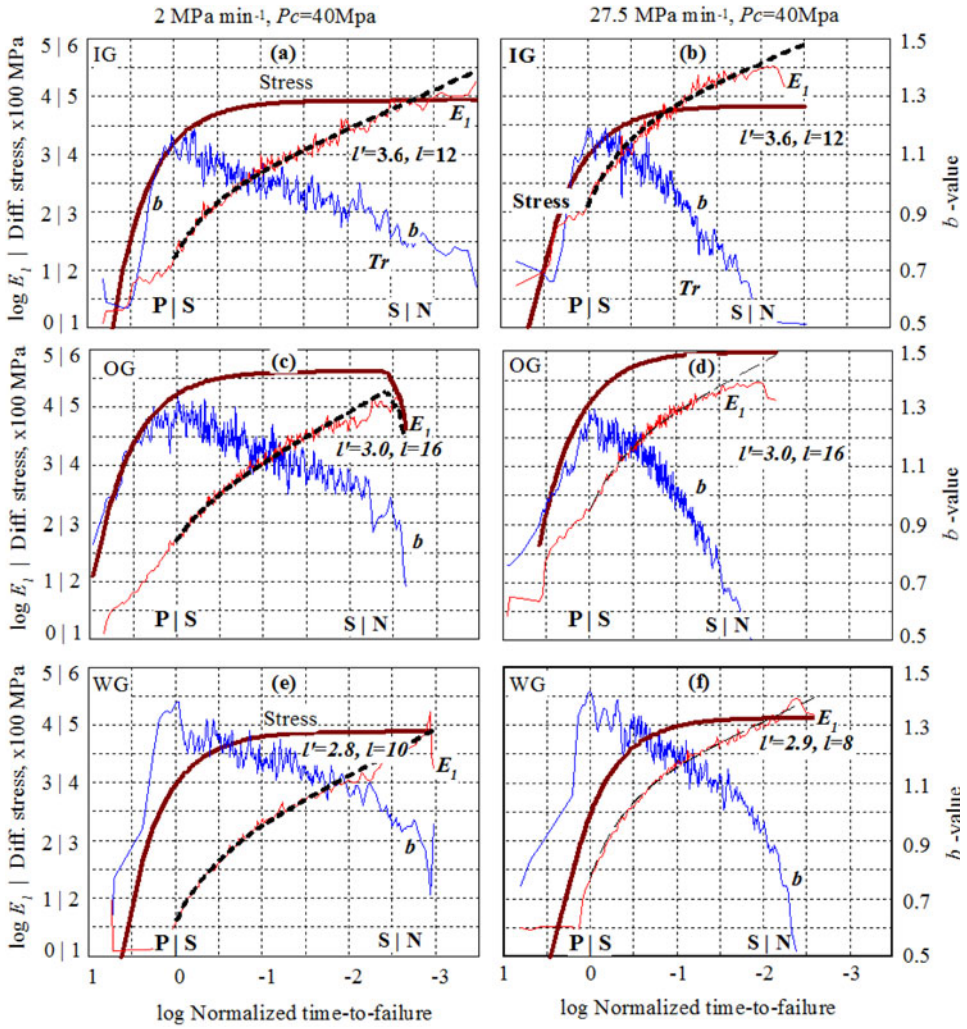

Fig. 1. Cumulative moment release (E) and b-value of AE in 3 granites having different grain size distribution, under two loading rates at 2 and 27.5 MPa/min. The time axis corresponds to the normalized time-to-failure in log scale, for presenting the acceleration of the evolution of the pre-failure damage. The dashed lines overlapping the moment release curves indicate the fit of the results of the sub-critical crack growth model with the energy release rate (E1). "P|S" and "S|N" denote the transitions from the primary to the secondary and from the secondary to the nucleation, respectively (from [32]).

increasing event rate and a rapidly decreasing b value until a global minimum around 0.5. Once the final fault was initiated at a key site, the faulting process will be governed by the accelerating growth of the fault and lead to a main event of extreme size.

4.2 Fracture of rocks with pre-existing weak planes

In crust, major earthquakes associate with rupture of pre-existing faults rather than fracture of intact rocks. Samples with pre-existing structures such as joints, foliations,

saw-cut and natural faults are thus more realistic model of natural earthquakes [5,9]. The 3-phase fracture process and the pre-failure damage laws are basically applicable to such cases. However, detailed evolution in each phase is strongly governed by the heterogeneities on the fault surface. In general, such samples exhibit fairly similar features to the fore- main- and after-shock sequence of natural earthquakes. These features are 1) small number of immediate foreshocks by which fault nucleation zones could be mapped; 2) the dimension of nucleation zone is normally a fraction of the main rupture dimension; 3) a lot of aftershocks concentrated on the shear fault; 4) stress drop due to the main rupture is of the order from a few 10 s to a few 100 s MPa; 5) b-value drops during foreshocks and recovers during the aftershocks.

It is worth to note that the critical nucleation zone size is also a function of loading conditions. As a extreme case, the failure process can be stabilized by controlling axial stress to maintain a constant rate of AE [1], resulting a nucleation zone size comparable with the sample dimension. However, under normal loading conditions such as constant stress rate loading and creep test, the critical nucleation zone size is normally a fraction of the sample dimension. This is the physical context that relates deviation from power laws to dragon-king: rupture beyond certain threshold size, i.e. the critical nucleation zone size, is hard to stop.

4.3 Fracture of strongly foliated rocks

Villaescusa et al. [39] presented a preliminary report on experimental results of systematical tests using two groups of samples of fine-grained rocks containing well developed foliations. Samples were drilled along different directions from two deep mines in Australia. These samples were subjected to 4 loading cycles while the confining pressure was kept constant at $5 \sim 20$ MPa. During the 4^{th} cycle, the axial stress was increased with a constant stress rate until the failure of the sample. A short aftershock phase was also recorded. On one hand, it is clearly recognized that the foliations have a governing role in all fracturing stages. On the other hand, samples with foliations favorably oriented for rupture, i.e., the angle between the foliation plane and the maximum stress axis is close to $30 \sim 40$ degree, demonstrate typical patterns of AE activity very similar with the fore- main- and after-shock sequence of natural earthquakes as aforementioned.

As an example, Fig. 2 shows continuous waveform record of acoustic emission during a 1-second period around the final shear fracturing of a test sample containing favorably oriented foliations. The stress drop due to the main rupture is ~ 20 MPa. Displacement along the main rupture is calculated to be ~ 0.35 mm from the measured axial displacement. Following the procedures described in Sect. 3 the equivalent radius of the fault and the equivalent earthquake magnitude are estimated to be $r \sim 0.8$ m and Mw ~ -1, respectively. For a comparison, the stick-slip event of a natural fault (created by triaxial compress in laboratory) in Westerly granite under 150 MPa confining pressure was estimated as to be Mw–0.32 [9].

As mentioned in the "Experiment and AE data" section, McGarr method results in an upper-bound of moment magnitude and thus using the actual moment of the ultimate failure is not fair. Using the estimated $r(0.8\,\text{m})$ and $\text{Mw}(-1)$ equation (10) results in $a = 4.7$. Again, this value is close to the typical values for earthquakes [38]. Now, it is ready to estimate the lower-bound of magnitude of the ultimate event by taking the sample dimension as the ruptured area in to (10). The resulted Mw is ~ -4. Fig 3 shows cumulative frequency-magnitude distribution of AEs. The main event is far from the Gutenberg-Richter power-law for fore- and after-shocks. AE hypocenter distribution demonstrates that the ultimate failure is preceded by a faulting nucleation stage with a critical nucleation size of $2 \sim 3$ cm. This fact indicates that rupture

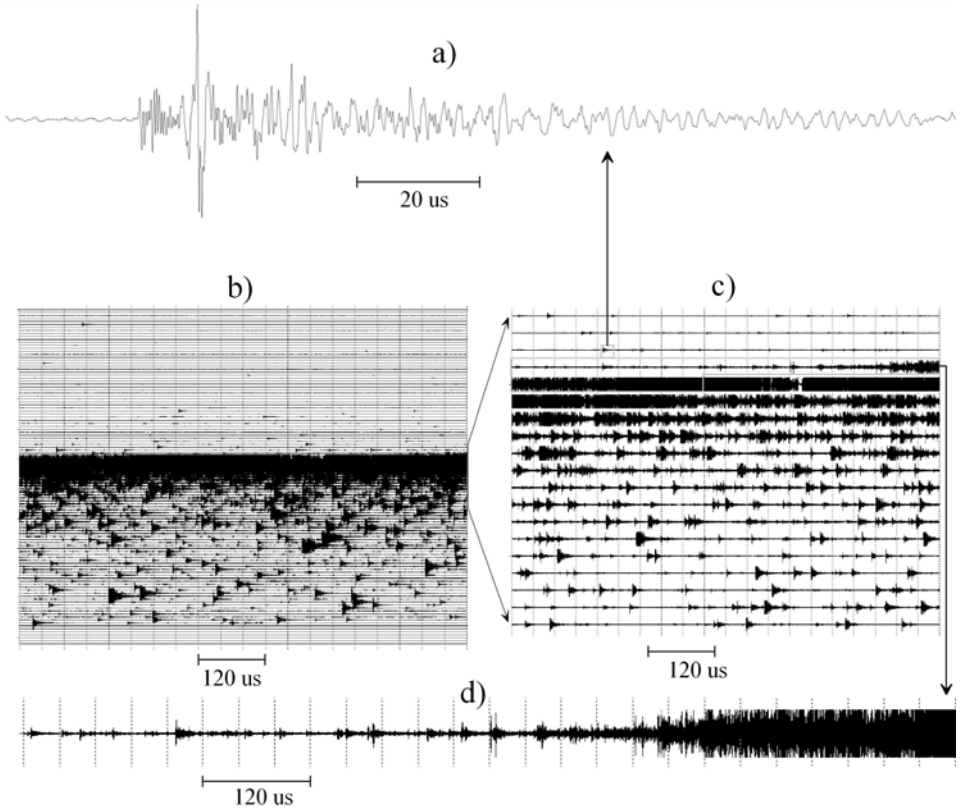

Fig. 2. Continuous waveform record of acoustic emission during the final shear fracturing of a strongly foliated rock sample. The main failure is preceded by progressively increasing foreshocks and followed by a lot of aftershocks.

beyond certain threshold size, that is in the order of $2 \sim 3\,\mathrm{cm}$, is hard to stop and thus results in a dragon-king event which has a magnitude greater (by $M2 \sim 3$) than the expected value from the Gutenberg-Richter power-law.

4.4 Rupture of naturally cemented joint in a granitic porphyry

Fig. 4 shows basic results of a triaxial compression test on a granitic porphyry containing rare pre-existing cracks and a naturally healed joint [40]. The finally ruptured fault coincides with the joint. AE events during the primary and secondary phases randomly clustered in the sample volume. The final fracture was initiated when background activity was quite low. A few immediate foreshocks were located in a small region near the top end of the sample. In this test, waveform from the mainshock was fortunately recorded on a quiet background, and thus its hypocenter and focal mechanism solution were determined. The nucleation zone, mapped by the foreshocks, demonstrates a critical dimension of $1 \times 3\,\mathrm{cm}^2$. The main event is located in the nucleation zone and shows a typical mechanism of "Wing-crack", initiated as a tensile crack and ruptured in shear mode as illustrated in Fig. 4-e. Again, the main event is a typical dragon-king.

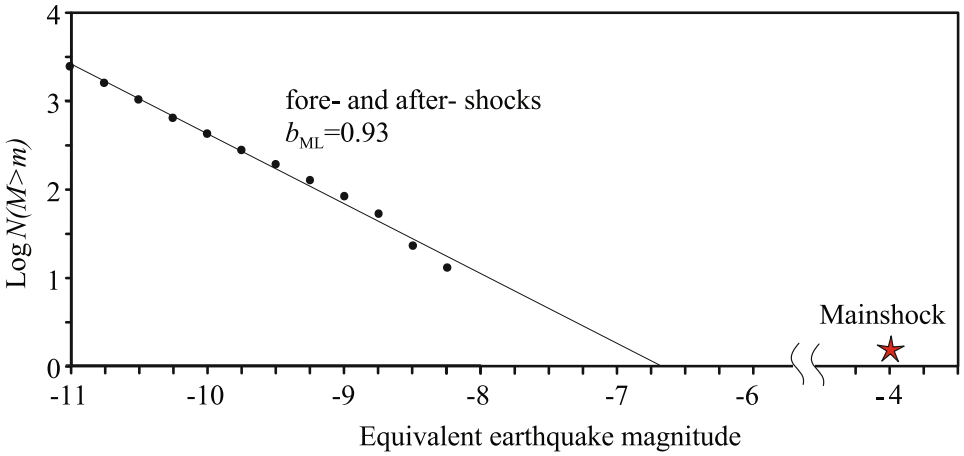

Fig. 3. Cumulative magnitude-frequency distributions of AEs obtained from the same test shown in Fig. 2. The mainshock has a magnitude significantly greater than that expected from the Gutenberg-Richter power-law relation for fore- and after-shocks.

4.5 Rupture of natural faults containing unbroken asperities

Lei [15] documented very interesting experimental results conserving the fracture of a shear fault containing several unbroken asperities in granitic porphyry. As asperities failed they transferred stress to neighboring asperities. The progressive failures of the coupled asperities characterize the quasi-static nucleation phase, preceding the dynamic rupture of the fault, and thus demonstrate the hierarchical nature of faulting. Figure 5 shows AE rates, b-values, and AE event magnitudes associated with the fracture of a major asperity having a dimension of $2 \sim 3$ cm. The fracture of individual asperities exhibit similar characteristics to the sequence for natural earthquakes, including foreshock, mainshock, and aftershock events. Foreshocks, initiated at the edge of the asperity, occur with an event rate that increases according to a power law of the temporal distance to the mainshock, and with a decreasing b-value (from ~ 1.1 to ~ 0.5). One or a few mainshocks then initiate at the edge of the asperity or the front of the foreshocks. The aftershock period is characterized by a remarkable increase in b-value and a decreasing event rate obeying the modified Omori law, which has been well established for earthquakes. It is very interesting that mainshocks show a magnitude extremely greater than the magnitude of AE events in either foreshocks or aftershocks (Fig. 6). The estimated magnitude (from the wave continuation time, see [15] for details) and source dimension (based on AE spectra, see [33] for details) for the largest main shock (indicated as e3 in Fig. 6) agrees well with that estimated for the mining-induced micro-earthquakes in a deep mine of more than 3 km depth in South Africa [10]. It is recognized that the Gutenberg-Richter power-law relation holds true for a magnitude range between -4.4 and -1.9 (a range filling up the gap between earthquakes and AEs in laboratory) [10].

5 Discussion and conclusion

In conclusion, the fracture of intact rocks or natural structures (joints, faults, foliations) under constant stress rate loading or creep conditions is generally characterized by three typical phases termed primary, secondary, and nucleation phases,

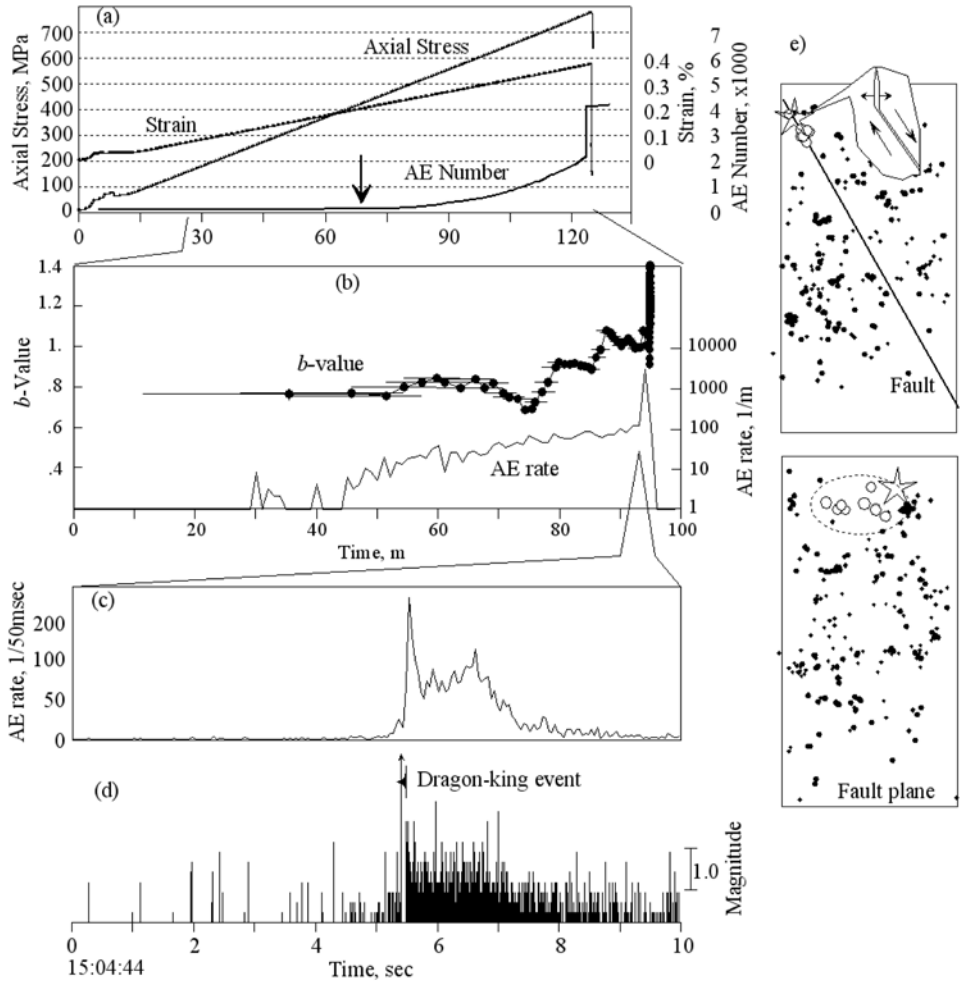

Fig. 4. The basic results of a triaxial compression test on a granitic porphyry having rare pre-existing cracks and a healed joint. (a, b) Axial stress, typical strain at 45 degrees with maximum stress, and accumulated AE number versus time. The arrow indicates the point of initiation of AE. (c) Close-up view around the dynamic fracturing. (d) Relative magnitudes are plotted in the lower panel. (e) AE hypocenters of the primary and secondary phases (black circles), immediate foreshocks (open circles), and the main event (star). ((a)–(d) Are updated from [40].)

respectively. The primary phase reflects the initial rupture of pre-existing microcrack population in the sample or in the fault zone. Sub-critical growth dominates the secondary phase. The nucleation phase corresponds to the initiation and accelerated growth of the ultimate fracture. The secondary and nucleation phases in both intact rock and faulted rock show power-law (of time-to-failure) increasing event rate and moment release. In total, pre-failure AE is more pronounced the more inhomogeneous the rock or the fault surface is. Under constant stress rate loading (including creep test where stress was kept constant), faulted samples demonstrate fairly similar features with the fore- main- and after-shock sequence of natural earthquakes including: 1) small number of immediate foreshocks by which fault nucleation zones could be

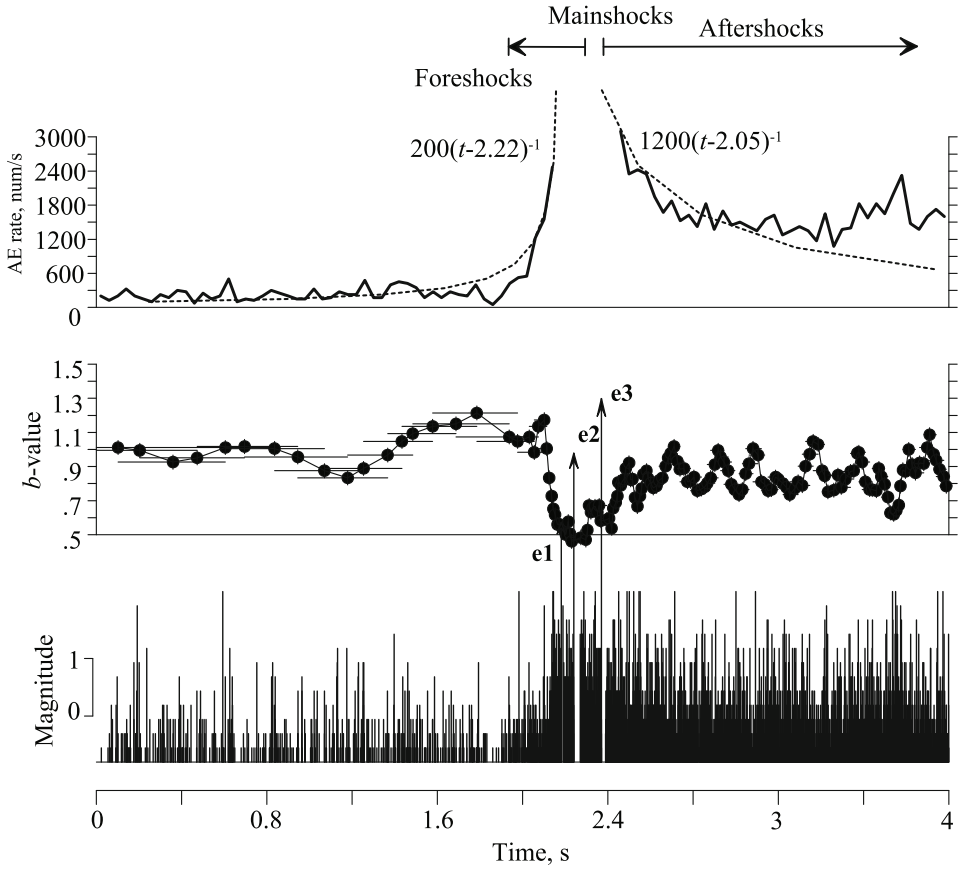

Fig. 5. AE rates, *b*-values, and AE event relative magnitudes associated with the fracture of an asperity on the fault surface. The *b*-values are calculated for sets of 100 events with a running step of 25 events by the maximum likelihood method. Dashed line denotes the power law of temporal distance from the main shock. Note that the fitting is rough due to background AEs and overlap with subsequent fracture of other asperities. (Updated from [15].)

mapped; 2) the critical nucleation zone size is normally a fraction of the main rupture dimension; 3) a lot of aftershocks concentrated on the shear fault ruptured during the main event; 4) stress drop due to the main rupture is at the order from a few tens to a few hundreds MPa. The power laws established for seismicity work pretty well for AE activity. All these results agree with the suggestion as discussed by Rice and Cocco [11], that laboratory measurements require no scaling but can be applied directly to the Earth to represent local fault behavior.

In all cases, the final failure of the test sample, or fracture of major asperities on the fault surface, normally leads to extreme events, dragon-kings, which are significantly deviated from the Gutenberg-Richter power-law relation for either foreshocks or aftershocks. There are at least two mechanisms may lead to dragon-kings: 1) The power-law (of time-to-failure) increasing event rate and moment release; and 2) Hierarchical fracturing behavior. In the 1st mechanism, the final failure corresponds to the end point of progressive occurrence of microcracks and thus the resulted dragon-king events can be interpreted as a superposition of many small events. While in the 2nd mechanism, event of extreme size is the results of fracture growth stepping from a lower hierarchy into a higher hierarchy on fault surface having asperities

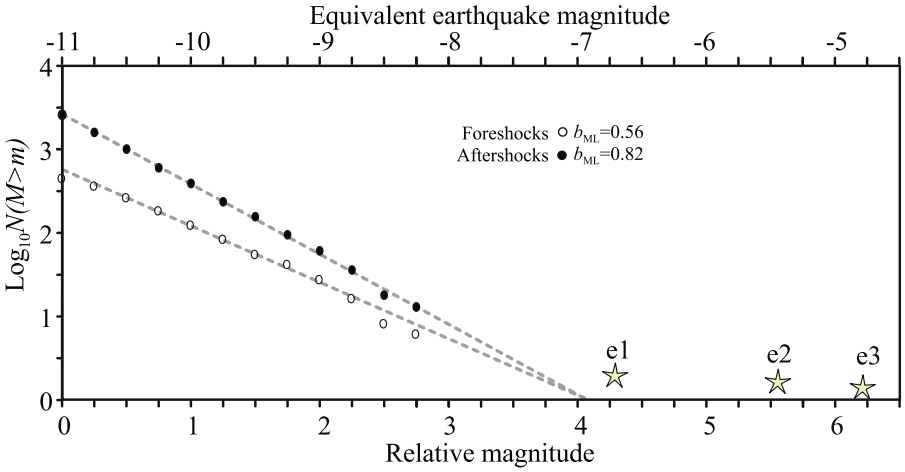

Fig. 6. Comparison of cumulative frequency-magnitude distributions of foreshocks with those of aftershocks. The magnitude of mainshocks is extremely greater than that predicted from the extrapolation of the Gutenberg-Richter power-law relation for either foreshocks or aftershocks.

characterized by hierarchical distribution (of size or strength) rather than fractal distribution. Both mechanisms suggest the same underlying physics that fracture in rocks is hard to stop beyond certain threshold, or in other words, the critical nucleation zone size.

A hierarchical distribution contains a characteristic scale in each hierarchy, whereas fractal distribution is scale-independent. Within an intact rock sample, the dominant grain size is a first order characteristic scale, and thus the sample contains 2 major hierarchies. Under stress, microcracks occurring within grain scales are govern by the gain scale heterogeneities, which are indeed fractal, and thus lead to chaotic behaviors power-laws in fracturing. However, once a fracture, which must be favorably located and oriented for rupture under the stress field, exceeded the dominant grain size, the fracture would grow faster than any others and would not stop until the strain is sufficiently released or met a stronger asperity. Similar scenario can be drawn for fault containing hierarchically distributed asperities.

This study is partly supported by the Japan Science Promotion Society (JSPS 21246134). The paper was improved in response to comments by two anonymous reviewers.

References

1. D.A. Lockner, J.D. Byerlee, V. Kuksenko, A. Ponomarev, A. Sidorin, Nature **350**, 39 (1991)
2. I. Main, P.R. Sammonds, P.G. Meredith, Geophy. J. Int. **115**, 367 (1993)
3. X. Lei, K. Kusunose, M.V.M.S. Rao, O. Nishizawa, T. Satoh, J. Geophys. Res. **105**, 6127 (2000)
4. A. Zang, F.C. Wagner, S. Stanchits, C. Janssen, G. Dresen, J. Geophy. Res. **104**, 23, 651 (2000)
5. X. Lei, K. Masuda, O. Nishizawa, L. Jouniaux, L. Liu, W. Ma, T. Satoh, K. Kusunose, J. Struct. Geol. **26**, 247 (2004)
6. X. Lei, T. Satoh, Tectonophysics **431**, 97 (2007)
7. B.D. Thompson, R.P. Young, D.A. Lockner, Geophys. Res. Lett. **32**, L10304 (2005)

8. B.D. Thompson, R.P. Young, D.A. Lockner, Pure Appl. Geophys. **163**, 995 (2006)
9. B.D. Thompson, R.P. Young, D.A. Lockner, J. Geophys. Res. **114**, B02205 (2009)
10. G. Kwiatek, K. Plenkers, M. Nakatani, Y. Yabe, G. Dresen, Bull. Seismol. Soc. Am. **100**, 3, 1165 (2010)
11. J.R. Rice, M. Cocco, *Seismic fault rheology and earthquake dynamics, in Tectonic Faults: Agents of Change on a Dynamic Earth*, edited by M. R. Handy, G. Hirth, N. Hovius (Dahlem Workshop 95, Berlin, January 2005 on the Dynamics of Fault Zones), chap. 5, (MIT Press, Cambridge, Mass, 2007), p. 99
12. B. Gutenberg, C.F. Richter, *Seismicity of the earth*, (Princeton Univ. Press, Princeton, N.J., 1954)
13. C.H. Scholz, Bull. Seism. Soc. Am. **58**, 399 (1968)
14. F. Liakopoulou-Morris, I.G. Main, B.R. Crawford, Geophys. J. Int. **119**, 219 (1994)
15. X. Lei, Earth Plan. Sci. Lett. **213**, 345 (2003)
16. Y.Y. Kagan, D.D. Jackson, Geophys. J. Int. **104**, 117 (1991)
17. T. Yamashita, L. Knopoff, Geophys. J. **96**, 389 (1989)
18. A. Sornette, D. Sornette, Tectonophysics. **179**, 327 (1990)
19. G. Ouillon, D. Sornette, Geophys. J. Int. **143**, 454 (2000)
20. A. Moura, X. Lei, O. Nishisawa, J. Mech. Phys. Solids **54**, 2544 (2006)
21. A. Moura, X. Lei, O. Nishisawa, J. Mech. Phys. Solids **53**, 2435 (2005)
22. J.C. Anifrani, C. Le Floch, D. Sornette, B. Souillard, J. Phys. I (France) **5**, 631 (1995)
23. D. Sornette, Phys. Rep. **29**, 239 (1998)
24. V.I. Yukalov, A. Moura, H. Nechad, J. Mech. Phys. Solids **52**, 453 (2004)
25. A. Bruce, D. Wallace, *Critical point phenomena: universal physics at large length scales*, edited by P. Davis, The New Physics (Cambridge Univ. Press, New York, 989), p. 236
26. G. Zöller, S. Hainzl, J. Kurths, J. Geophys. Res. **106**, 2167 (2001)
27. C.G. Bufe, D.G. Varnes, J. Geophys. Res. **98**, 9871 (1993)
28. C.G. Bufe, S.P. Nishenko, D.J. Varnes, Pure Appl. Geophys. **142**, 83 (1994)
29. D.D. Bowman, G. Quillon, C.G. Sammis, A. Sornette, D. Sornette, J. Geophys. Res. **103**, B10, 24359 (1998)
30. S.C. Jaume, L.R. Sykes, Pure Appl. Geophys. **155**, 279 (1999)
31. Y.S. Tyupkina, R. Di Giovambattista, Earth Planet. Sci. Lett. **230**, 85 (2005)
32. X. Lei, in *Fractal Analysis for Natural Hazards*, edited by G. Cello, B.D. Malamud, vol. 261 (Geological Society, London, Special Publications, 2006), p. 11
33. X. Lei, K. Kusunose, T. Satoh, O. Nishizawa, Phys. Earth Planet. Inter. **137**, 213 (2003)
34. A. McGarr, J.B. Fletcher, Bull. Seismol. Soc. Am. **93**, 2355 (2003)
35. J.D. Eshelby, Proc. Royal Soc. London, Ser. A **241**, 1226, 376 (1957)
36. J.B. Walsh, J. Geophys. Res. **76**, 8597 (1971)
37. T.C. Hanks, H. Kanamori, J. Geophys. Res. **84**, 2348 (1979)
38. D.J. Dowrick, D.A. Rhoades, Bull. Seismol. Soc. Am. **94**, 776 (2004)
39. E. Villaescusa, X. Lei, O. Nishizawa, T. Funatsu, Austr. Mining Technol. Conf. **1-14**, 27 (2009)
40. X. Lei, K. Kusunose, O. Nishizawa, A. Cho, T. Satoh, Geophys. Res. Lett. **27**, 1997 (2000)